Final Technical Report

Project Title:	"Flexible Ultra Moisture Barrier Film for Thin-Film Photovoltaic Applications"
Covering Period:	August 1, 2009 to July 31, 2012
Date of Report:	October 30, 2012
Recipient:	E.I. du Pont de Nemours and Company
Award Number:	DE-EE-0000588
Working Partners:	N/A
Cost-Sharing Partners:	N/A

Contacts:

David Dean
Phone: (302)-695-1697
Fax: (302)-695-3366
Email: david.m.dean@usa.dupont.com

Neil Washburn
Phone: (302)-695-3196
Fax: (302)-695-3366

DOE Project Contact: DOE Field Project Officer - Doug Hall

Project Objective:

Design, fabricate and operate a continuous ALD deposition process by means of a prototype system, followed by construction and optimization of a pilot system to demonstrate the potential for commercial production of flexible high moisture barrier ALD-on-plastic film.

Background:

Flexible Thin-film photovoltaic (TFPV) is a low cost alternative to incumbent c-Si PV products as it requires less volume of costly semiconductor materials and it can potentially reduce installation cost. Among the TFPV options, copper indium gallium diselenide (CIGS) has the highest efficiency and is believed to be one of the most attractive candidates to achieve PV cost reduction. However, CIGS cells are very moisture sensitive and require module water vapor transmission rate (WVTR) of less than $1x10^{-4}$ gram of water per square meter per day ($g\text{-}H_2O/m^2/day$). Successful development and commercialization of flexible transparent ultra moisture barrier film is the key to enable flexible CIGS TFPV products, and thus enable ultimate PV cost reduction.

At DuPont, we have demonstrated at lab scale that we can successfully make polymer-based flexible transparent ultra moisture barrier film by depositing alumina on polymer films using atomic layer deposition (ALD) technology. The layer by layer ALD approach results in uniform and amorphous structure which effectively reduces pinhole

density of the inorganic coating on the polymer, and thus allow the fabrication of flexible barrier film with WVTR of 10^{-5} g-H_2O/m^2/day.

Currently ALD is a time-consuming process suitable only for high-value, relatively small substrates. To successfully commercialize the ALD-on-plastic technology for the PV industry, there is the need to scale up this technology and improve throughput.

SOPO Status:

At the close of the project (July 31, 2012), the following tasks from the Statement of Project Objectives (SOPO) were completed:

Task 1.1 Complete the design of the prototype (as previously reported)

Task 1.2 Fabricate the prototype (as previously reported)

Task 2.1 Establish testing protocol (as previously reported)

Task 5.2 Establish the grade for PET film and secure supply (as previously reported)

At the end of the contract period, work was focused on producing film from the upgraded prototype and continuing the work of Task 2.2: Determining the Process Window.

The prototype failed to produce an ultra-barrier film by the close of the project.

Summary of Technical Work

Concept

The essential idea for the DuPont coating head is illustrated in Fig. 1. The coating head shown is a sketch of our prototype, which was designed to provide only one ALD cycle. A coating head designed for use in manufacturing would have more of a square aspect ratio: its length in the machine direction is likely to be similar to its width in the transverse direction.

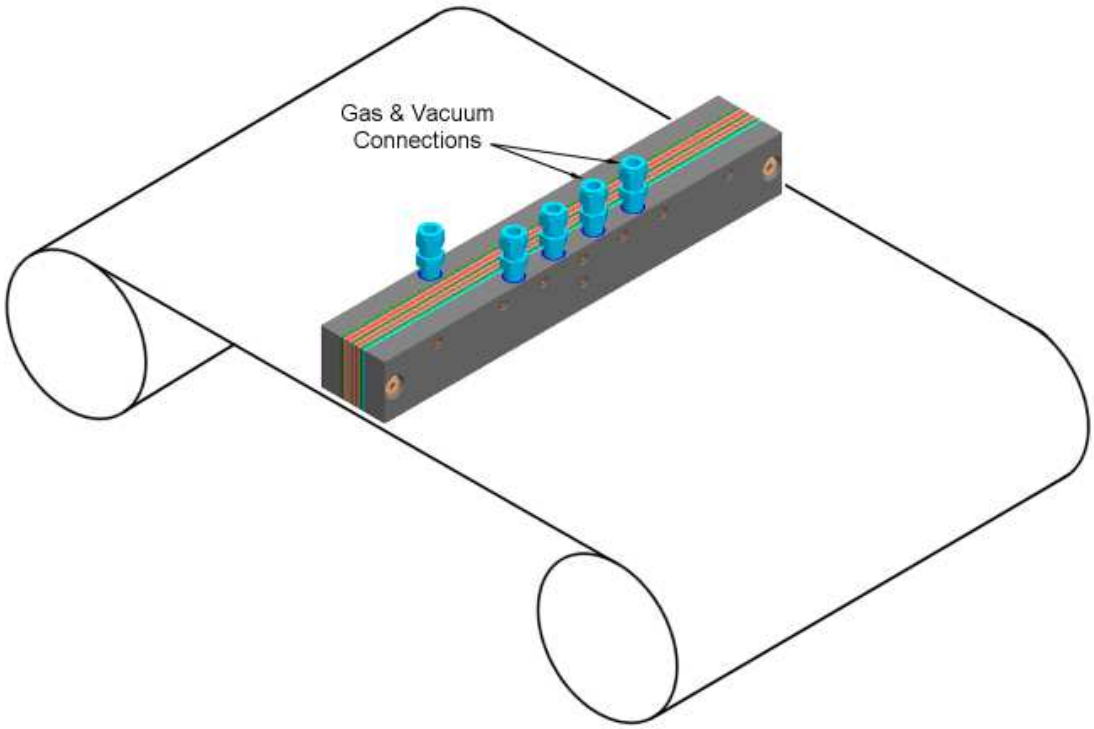

Figure 1 Simplified sketch of the DuPont coating head.

A cross-section of the head is shown in Fig. 2. Identical metal plates define a series of channels that either deliver or withdraw gas. The figure shows the channels required to build a single cycle of oxide on the surface. The pattern would simply be repeated to provide the required number of layers in a production head. A raised ridge on each plate creates a small gap with the adjacent plate, which serves to limit the flow and ensure an even distribution of gas across the width of the web.

The head has a very simple operating concept. A section of the PET web passes underneath a precursor delivery channel, allowing precursor to react with the surface. This section then moves under a so-called vacuum channel where un-reacted precursor gas is drawn away from the web surface, aided by the pure nitrogen purge flow emanating from the next channel. The web then passes an upstream vacuum channel and under the delivery channel for the other precursor, where the reaction is completed. By stacking additional plates, this pattern can be repeated as many times as necessary to complete a barrier coating in a single pass.

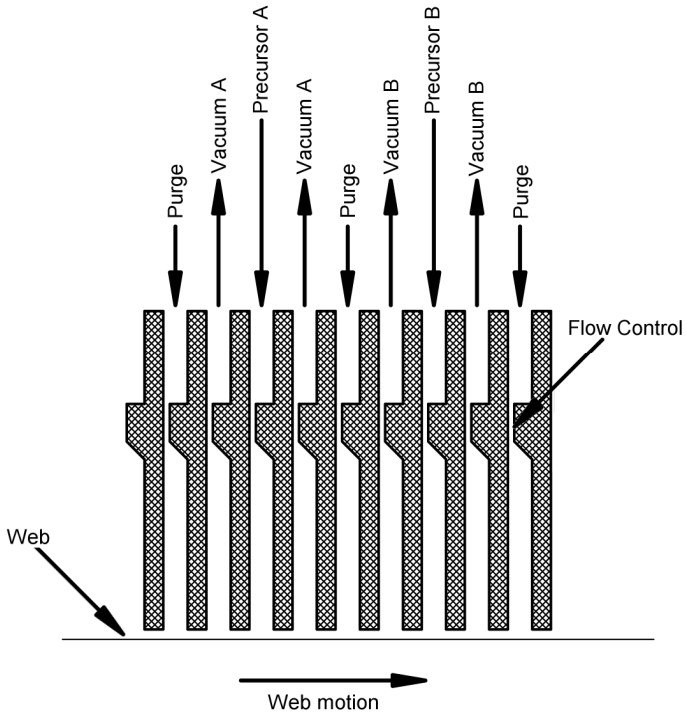

Figure 2 Schematic cross-section of the DuPont ALD head.

Modeling

A feasibility analysis of this coating head was performed using numerical modeling. Fig. 3 summarizes the model's results for coating TMA. The inset shows the steady state coating profile as a function of precursor concentration. The vertical axis shows the fraction of the surface that has reacted with the incoming precursor gas, while the horizontal axis shows the position under the coating head. The channels in the deposition head are sketched in the background. The web enters the figure at the left edge, un-coated, starts to pick up a coating at about x = 6 mm (in the gap under the plate that separates the precursor delivery channel from the upstream vacuum channel). The coating builds over a rather short distance, and the film exits at the left, fully coated—provided there is enough input TMA. The main graph in the figure shows the final coating thickness as a function of the input TMA concentration. The coated thickness is independent of input concentration (as expected for ALD, and as guaranteed by the mathematics of the simulation) until the TMA concentration falls below about 0.2%.

Figs. 4 and 5 show that the coating process is relatively insensitive to either web speed or separation between the output face of the head and the web. In the first figure, one can see that the point at which most of the deposition occurs shifts steadily downstream as the substrate velocity increases, but in all cases a complete coating is formed. In the second figure, the gap is increased from the initial 50 µm to 125 µm in increments of 25 µm, with only a minimal impact on the coating profile.

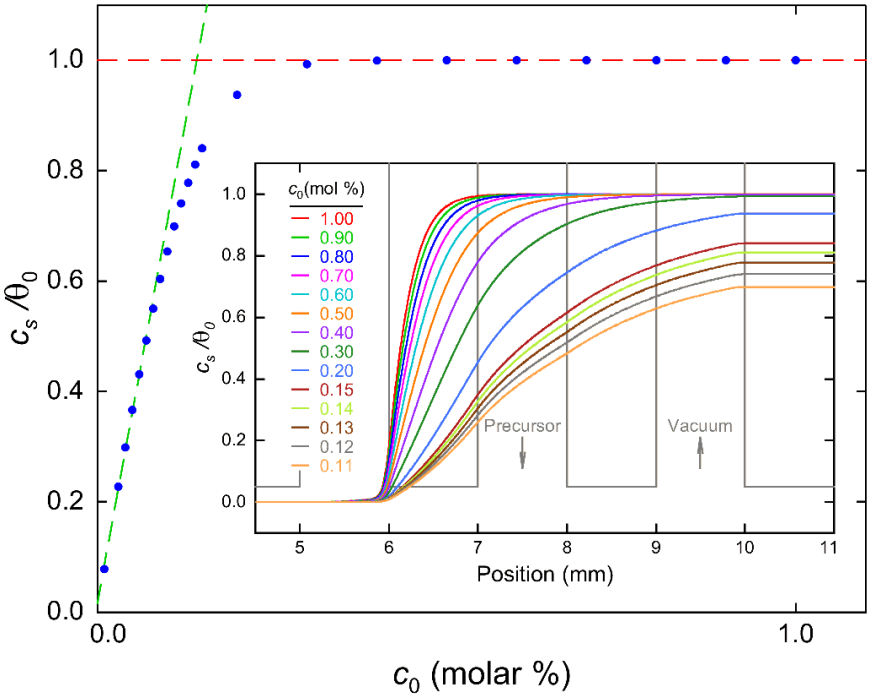

Figure 3 Surface coverage as a function of input precursor concentration. The inset shows the deposition profiles in the steady state for input concentration c_0 greater than 0.1%

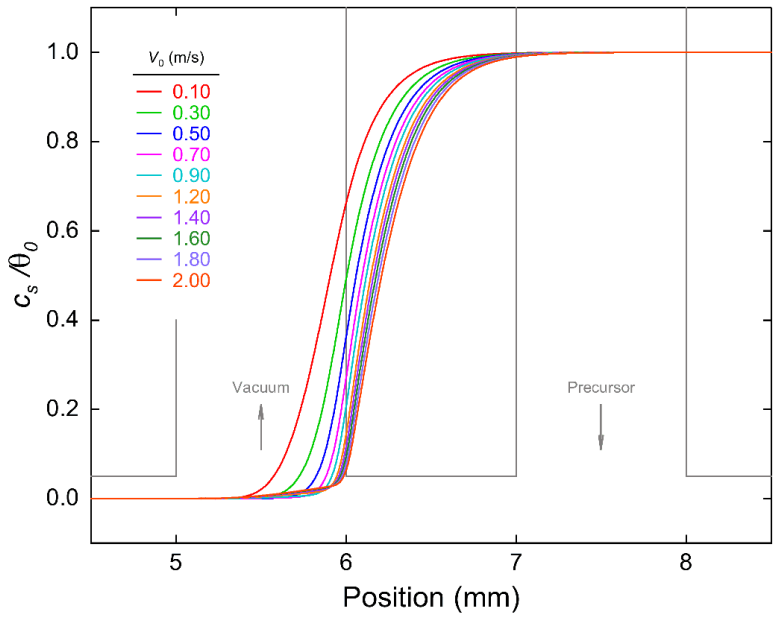

Figure 4 Surface deposition profile as a function of substrate velocity, V_0.

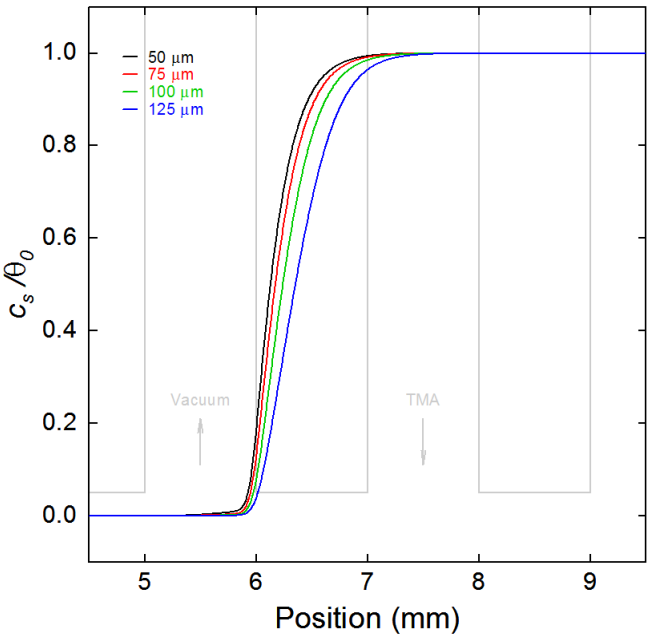

Figure 5 Surface coverage as a function of gap height.

Although Fig. 5 implies that the gap height between the coating head and the web is of no concern, that is not actually the case. A critical requirement for a functioning coating head is precursor confinement:

The same model was used to study the water reaction step. The results are shown in Fig. 6. Comparison with Fig. 3 shows that the deposition actually occurs more quickly (over a shorter distance along the substrate) for water than for TMA, in spite of the slower surface rate. This implies that deposition is occurring in a regime where diffusion of precursor to the surface is still the limiting factor.

Confinement

Fig. 5 implies that the coating process is insensitive to the distance between the coating head and the web. This is only true if one neglects interactions between adjacent coating steps. In the TMA-water ALD process, reactions can occur in the gas phase, resulting in chemical vapor deposition (CVD) instead of ALD, and a presumed reduction in barrier quality. If precursor A is not "confined", then it can migrate downstream and react in the gas phase with precursor B. To investigate confinement, we used a large model that included two precursor delivery channels, along with the attendant vacuum and purge channels. This model reflects the actual coating bar used in the prototype coating system, and includes extra vacuum channels intended to reduce the possibility of precursor escaping to the surrounding atmosphere. We injected precursor into the A delivery channel and measured the amount of precursor present in the first (upstream) B vacuum channel. The calculation was repeated for various gap heights. The result is shown in Fig. 7. The concentration has been normalized by the input amount. One can see that at a gap height of 100 µm the concentration of A in the B vacuum channel is extremely low, but that it rises quite rapidly as the gap is increased. The model was also used to show that this problem

could not be remedied by increasing the purge flows. The only way to maintain confinement is to keep the gap height at 100 µm or less.

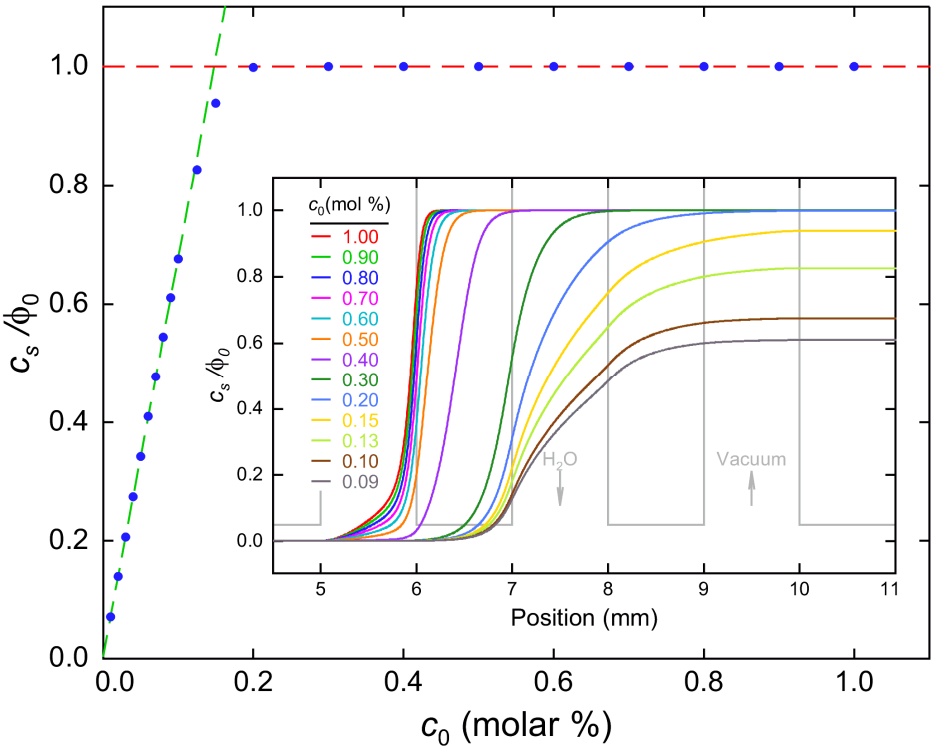

Figure 6 Coverage as a function of input water concentration. The inset shows the actual steady state coating profiles.

solution superimposed.

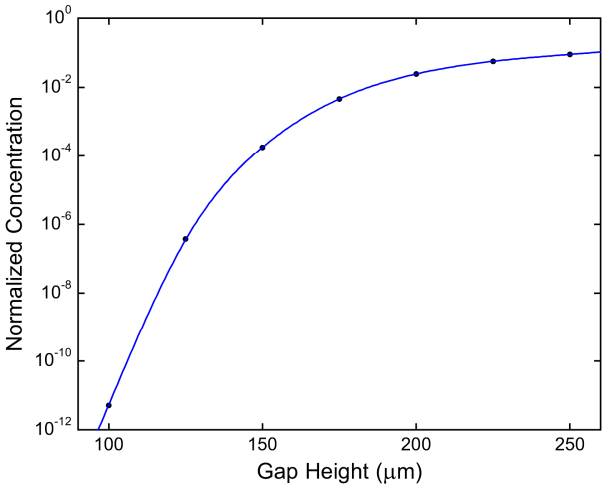

Figure 7 Fractional concentration of precursor appearing in the upstream B vacuum channel.

Construction Details

The strategy to construct an actual coating head that mirrors that in the model was to use a stack of machined metal plates separated by Kapton® gaskets. An exploded view is shown Fig. 8. Each plate in the figure is color coded to indicate the function of the channel it defines: green indicates purge gas delivery, pink indicates fluid removal ("vacuum") channels, and darker red and brown indicate precursor delivery. The blue plate is an "end effect" fluid removal channel which would not be part of the repeated plate structure in a production head. The corresponding channel at the other end of the head is provided by cuts in the large end block.

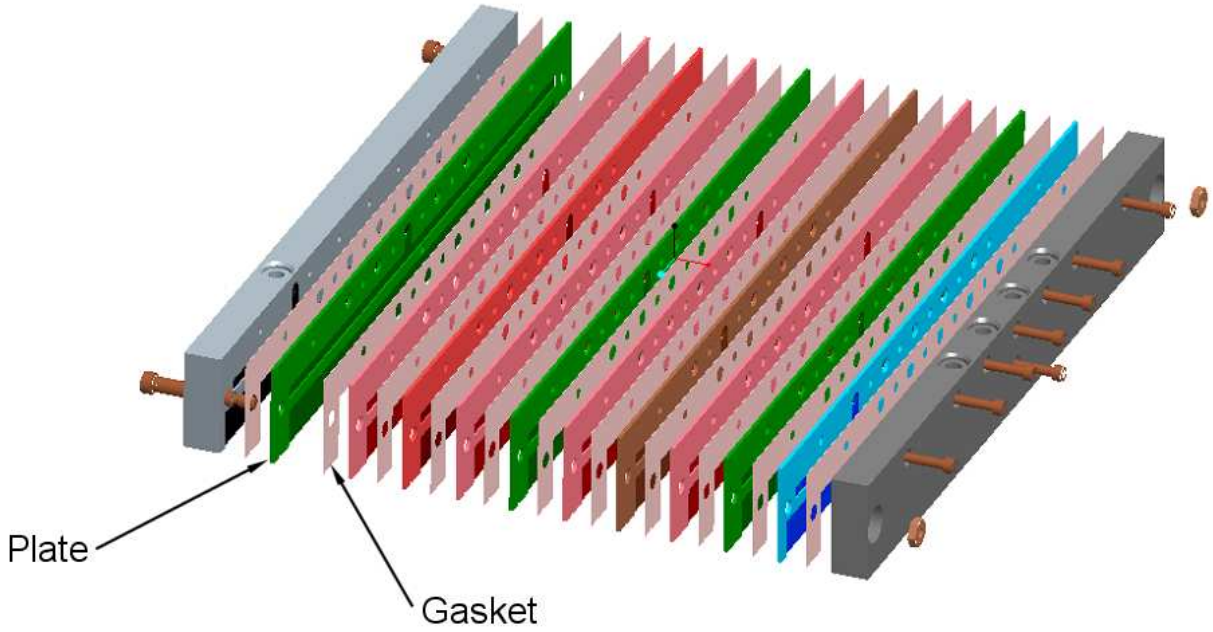

Figure 8 Exploded view of the prototype coating head showing the individual plates and the gaskets that separate them.

Fig. 9 shows and individual plate and gives a clearer idea of the manufacturing method. The plate material is 3/32" ground stock which has been cut down to half the original thickness in regions "S" and "F". These cut away regions form the fluid channel, and the raised "R" section forms the flow control element. The "H" holes are used to assemble the head, but the "G" holes stack to form pipes for the delivery and removal of the gases. One of the "G" holes is designated a "U" hole, because the cut away region extends up to connect a gas supply pipe to the channel defined by this plate.

Fig. 10 shows one of the Kapton® gaskets. The actual gasket thickness is 0.002 inches, which defines the width of the flow control element. Note that the gasket has the same shape as the parts of the plate that have *not* been thinned, except in the "R" region. The gaskets were manufactured by compressing 15 or 20 sheets Kapton® between two stiff boards and using a water jet to cut all of them in a single operation.

Because of the strict requirements on the gap height, some care needed to be taken in the design and assembly of the head. Some of the "H" holes in Fig. 9 accommodate ground dowel pins. Once assembled, the output face of the head was precision ground. The dowels allow the head to be taken apart and reassembled without losing that precision.

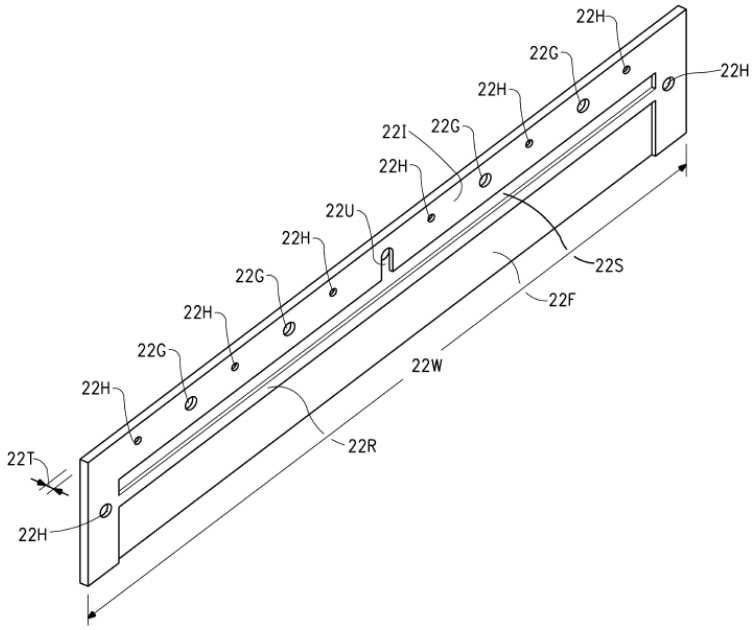

Figure 9 Illustration of a single plate showing the cut away regions that define the channel and the holes which align to form the fluid delivery and removal pipes.

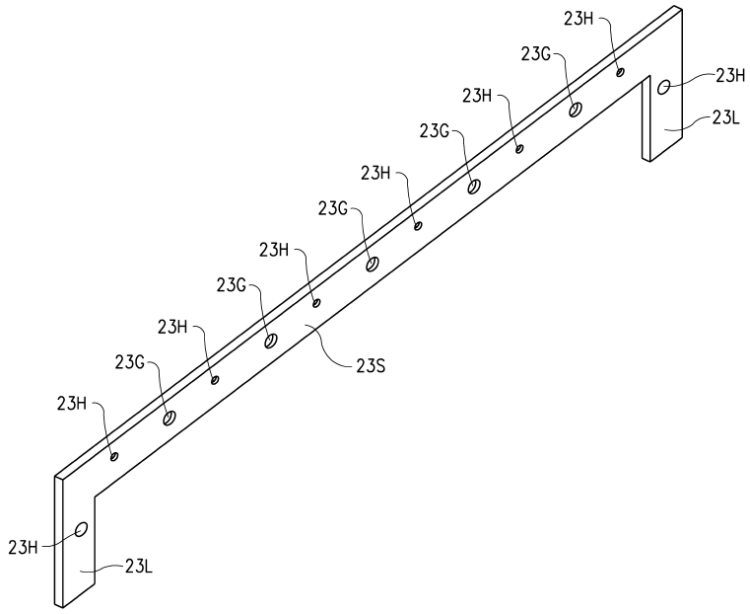

Figure 10 Illustration of the gasket which separates the various plates. All the gaskets are identical.

Fig. 11 shows a cross-section of the head through the N_2 (purge gas) delivery pipe. This figure gives a clear idea of how the plates and gasket stack, and how connections are made from the pipes to the channels.

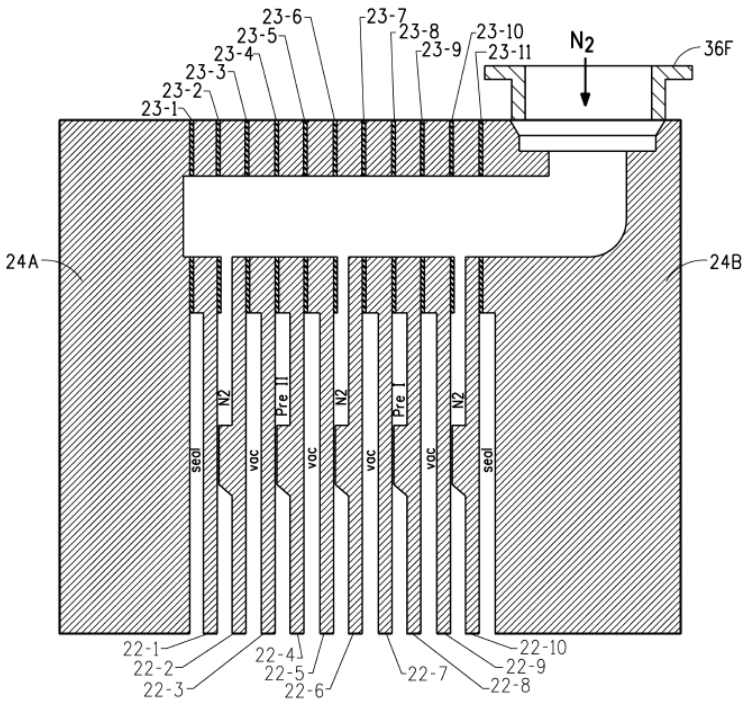

Figure 11 Cross-section illustration of the assembled head showing the stacking of the plates and gaskets. The channels labeled "seal" in the figure are the "sweep" vacuum channels.

Chamber Design

Although the deposition process runs at atmospheric pressure, the pyrophoric nature of the TMA requires that this atmosphere be free of oxygen and water. The chamber provides the necessary isolation. It is no more than a large aluminum box, as shown in Fig. 12, with a removable front. While the chamber does not have to support a vacuum, it has to be sealed "vacuum tight" in order to keep ambient oxygen and water out. For safety, the chamber has both over-pressure and under-pressure relief devices designed to open at a pressure differential of 2 psi. These are very simple devices, essentially heavy trap doors, held closed only by gravity, and sealed with an o-ring. In normal operation, the chamber is maintained at a pressure 50 mbar above atmospheric.

Drum Design

A manufacturing process using this head design would have to be able to deposit on a moving web. In order to focus on the head and the coating process, rather than on web handling, we simulate the moving web with a rotating drum, illustrated in Fig. 13. This approach allows us to deposit a coating of arbitrary thickness using a head that deposits only one cycle of ALD. The drum is 10" in diameter, and holds down a (22" × 30") piece of PET by vacuum. One end of the drum is supported on a roller bearing. The other is supported by a complex rotary union that provides a seal to chamber wall, a vacuum connection to the interior of the drum, electrical

connections to the heaters and thermocouples embedded in the drum wall, and a drive shaft for drum rotation. After considerable effort, we achieved a total indicated run-out (TIR) of 0.0008".

Figure 12 The chamber with the door secured.

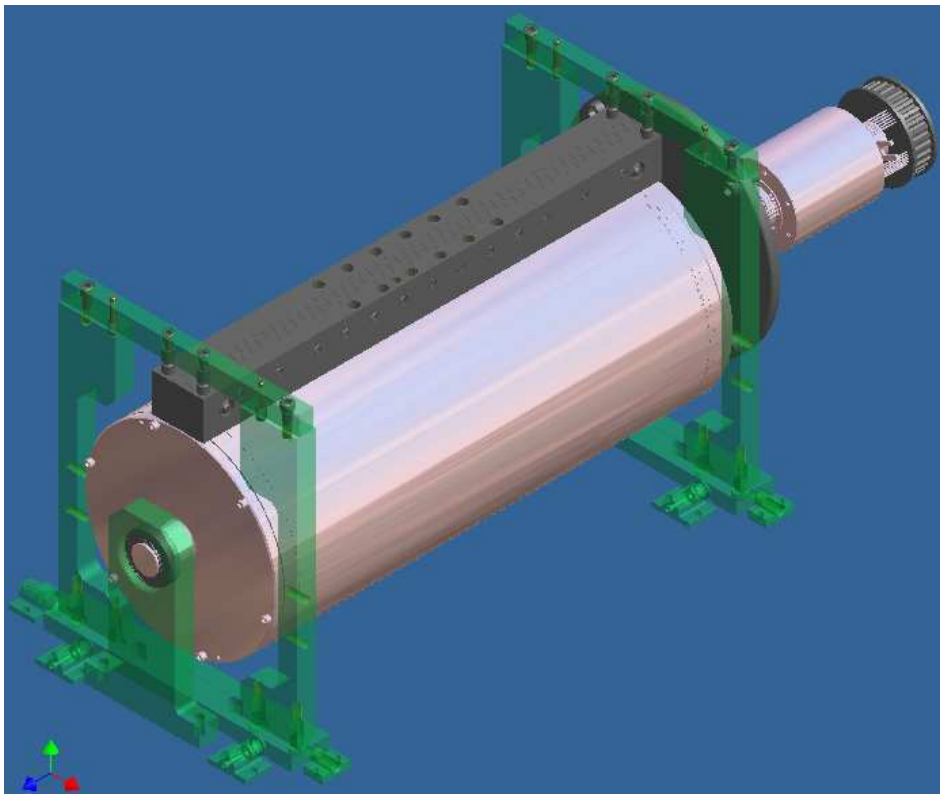

Figure 13 The drum, coating head, and coating head supports.

Because of thermal expansion, setting the required gap between the head and the drum requires some effort. (The output face is not flat as in Fig. 11, but has been ground to match the curvature of the drum.) Coarse shims under the crossbars that hold the head provide a rough adjustment. Fine adjustment must be made with the drum, head, and head supports at operating temperature (~100 C). The gap is measured with feeler gauges (with a piece of PET on the drum), and set to the desired height by adjusting the screws that hold the cross-bars to the support posts. This final adjustment occurs by bending the crossbars by a small amount. When the system is hot, fine trimming of the gap can be done by changing the temperature of the support posts. There is enough range in this last adjustment to maintain a constant gap even as the drum and head temperature are raised to 120 C. Rotation of the drum is driven by a servo motor under computer control.

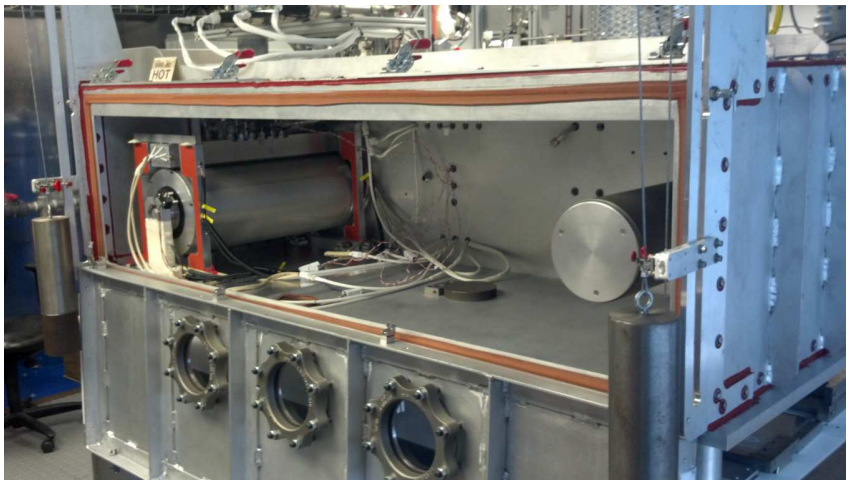

Figure 14 The chamber with the door lowered, showing the drum system at the far end.. The cylinder at the near end of the chamber is part of a system to allow deposition on larger samples.

Analysis Methods

Sample films produced using the prototype coating system were assessed using the following techniques.

Sulfuric Acid Test The oxide layer is covered in concentrated H_2SO_4 for 60 seconds and then rinsed with deionized water. The acid penetrates pinholes, scratches, and other damage and attacks the PET. This makes macroscopic damage easily visible to the naked eye and pinholes observable with a microscope at low magnification (50X).

UV Optical Interferometry This instrument, made by Filmetrics, gives a value for the thickness of the film. It has the advantage that it is fast and easy, which allows immediate feedback, as well as thickness measurements across the whole width of the film. The technique does require optical models for both the PET and the Al_2O_3, so the accuracy of the measurement is dependent on the accuracy of the model. Variations in the index of refraction of the deposited oxide will result in spurious variations in the as-measured thickness.

X-ray Reflectivity This technique fits the density and thickness of the film simultaneously, and is not dependent on a model for the PET substrate, and is thus considered more accurate for thickness. It also returns a value for the film density, which the optical method does not.

WVTR Measurement of the water vapor transmission rate (WVTR) using a MOCON Aquatran gives the most direct measure of barrier performance, but attempting to measure a poor quality sample can shorten the life of the instrument. As a consequence, we have submitted only a few samples for this test, generally those that were found to have a very small density of pinholes via the sulfuric acid test.

Photoelectron Spectroscopy Known locally as ESCA (electron spectroscopy for chemical analysis) provides a detailed picture of the elements present in the film. The instrument available has an ion beam for depth profile, so it is possible to look at the relative concentrations as a function of depth in the film.

Data Collection

Fig. 15 shows how we take the film from the drum and cut it into 20 coupons for analysis. Four coupons (typically A-1 through A-4) are sent for measurement by Filmetrics at three locations on each coupon. The locations are arranged so that we get back twelve measurements of the thickness evenly spaced across the width of the film. Four more coupons (typically B-1 through B-4) are cut down into 1" wide strips and sent for x-ray reflectivity measurements. The strip is cut so that the x-ray measurement is performed on what was the center of the coupon. Finally, four coupons (C-1 through C-4, usually) are send for acid treatment and pinhole counting.

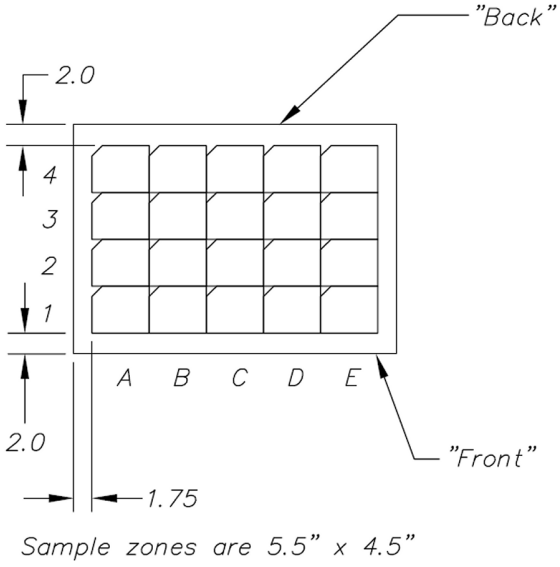

Figure 15 The standard scheme for cutting each film into coupons for analysis.

In order to ensure reasonable statistics on the pinhole measurements, and prevent unintentional bias in the counting, we use a standard mask with ten holes, as in Fig. 16. The number of pinholes visible at each location is counted, and the resulted is normalized by the area of the field of view (0.18 cm^2) to give a pinhole density.

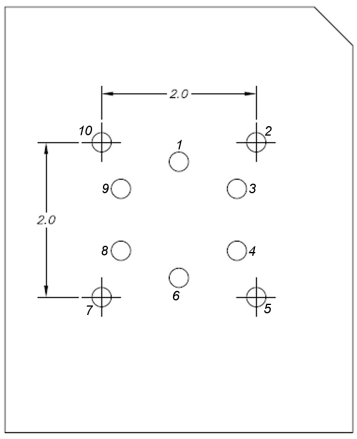

Figure 16 Approximate pinhole counting locations as determined by our standard mask.

Results

An experiment to investigate the effect of precursor concentration ratio was carried out under "standard" conditions, as indicated in Table 1:

Table 1

Drum Speed	0.5	m/s
No. of Cycles	300	
Deposition Temperature	100	C
Purge Flow Rate	10.5	SLPM
Precursor Flow Rate	1.75	SLPM
TMA concentration	0.2	mol %
Substrate	ST504	

The water concentration was varied from 0.05 to 0.5 molar %. The expected behavior is that the growth per ALD cycle would increase quickly with the concentration of water, and then flatten out once the concentration was high enough to satisfy the ALD stoichiometry. Fig. 17 summarizes the results. As one can see from the upper part of the figure, there is a change in the slope of the growth rate at a water concentration of approximately 0.2%, This break is not particularly sharp, however, and the ultimate growth rate achieved is well below the target of just below 1 Å/layer.

Also shown in the figure is the density and pinhole rate obtained for the samples. The density is essentially unaffected by the changing precursor ratio, and remains constant at about 2.6 g/cm^3. Our ALD films (produced by other methods) that perform as good barriers have a density of 2.8 g/cm^3, as indicated by the target line.

At low water concentrations, the pinhole density appears to drop linearly as the water concentration is increased towards 0.2%, but at high concentrations appears to be more or less random. Subsequent experiments continued to show large spreads in the pinhole rates, forcing the conclusion that the linear behavior seen in the figure was a statistical fluke.

Also shown in the figure is the target pinhole rate of 1 pinhole/cm^2. ALD films produced by other method have been repeatedly shown to have ultrabarrier properties and to have a WVTR too small for the MOCON Aquatran to detect. Samples from two experiments with low pinhole rates were submitted for MOCON testing, and the average WVTR measured is shown on the figure. Clearly, these are not ultrabarrier films.

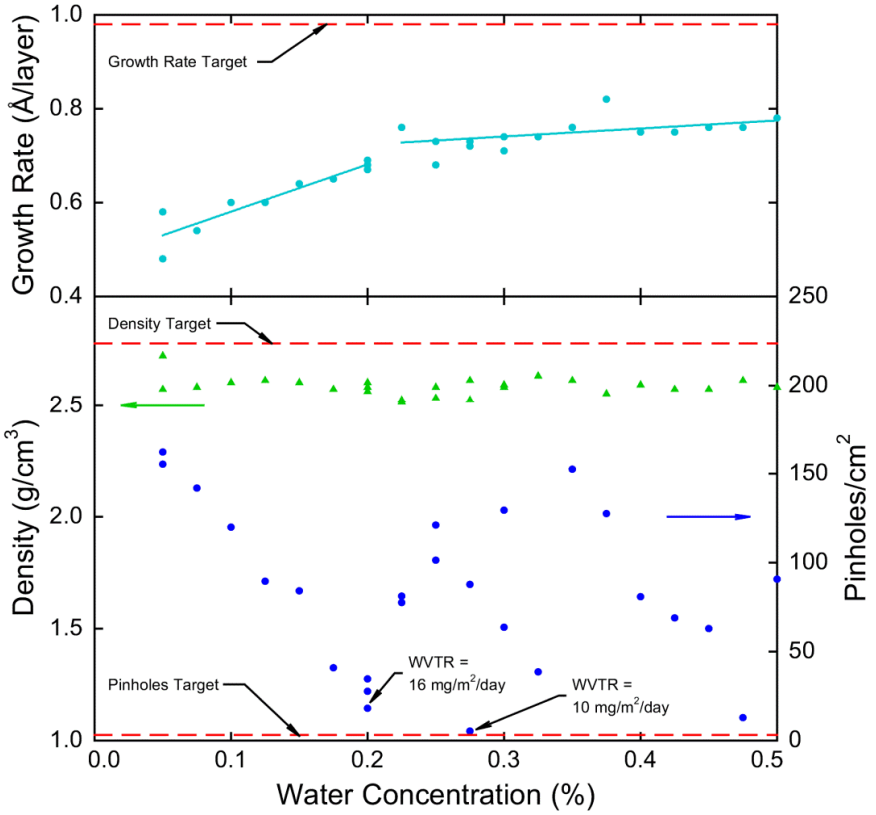

Figure 17 The growth rate per cycle (as determined by x-ray reflectivity), as well as the density and pinhole rate for 26 different samples as a function of water precursor concentration.

In a separate experiment, a 400 layer sample was made using TMA and water precursor concentrations of 0.1%. (The remainder of the sample conditions matched those in Table 1.) The resulting film had a thickness of 40 nm, and had a WVTR too small to be detected by the MOCON Aquatran. Subsequent testing under 85 ºC/85% relative humidity conditions showed that these films failed in less than 100 hours. Films with ultrabarrier properties last well beyond 1000 hours in these conditions.

A second experiment was conducted to investigate the importance of overall precursor flow. The standard conditions for this experiment are listed in Table 2. The total precursor flow was varied from 1.5 SLPM to 4 SLPM, with the flow and concentration equal for both precursors. The Purge flow was set to three times the precursor flow for each film. The results of this experiment are illustrated in Fig. 18. The film growth rate, density, and pinhole rate appear to be independent of the amount of precursor in this regime.

Table 2

Drum Speed	0.5	m/s
No. of Cycles	300	
Deposition Temperature	100	C
TMA concentration	0.2	mol %
Water concentration	0.2	mol %
Substrate	ST504	

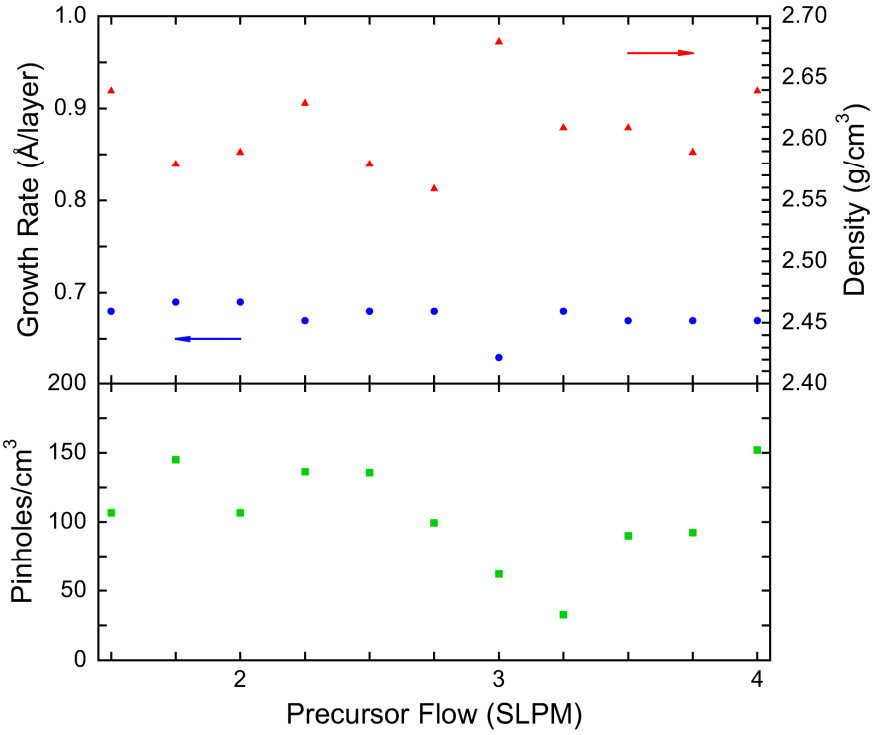

Figure 18 The growth rate per cycle, as well as the density and pinhole rate for 11 different samples as a function of precursor flow.

We also investigated the effect of deposition temperature, using standard conditions as shown in Table 3. The deposition temperature was varied from 100 ºC to 120 ºC, with the results shown in Fig. 19. This experiment is interesting, because unlike the previous ones, there appears to be a clear trend in both density and pinhole rate. Interestingly, these trends appear uncorrelated, or possibly anti-correlated. Given that each temperature was repeated, we have reasonable confidence in both trends. The experiments were performed by generating a list of 10 temperatures (5 by 2 replicates) and randomizing the lists so as to avoid systematic effects. Of course, even at the minimum, the pinhole rate is unacceptably high, but it remains a challenge to understand what drives this aspect of the experiment.

Table 3

Drum Speed	0.5	m/s
No. of Cycles	300	
Precursor flow rate	3	SLPM
Purge flow rate	6	SLPM
TMA concentration	0.2	mol %
Water concentration	0.2	mol %
Substrate	ST504	

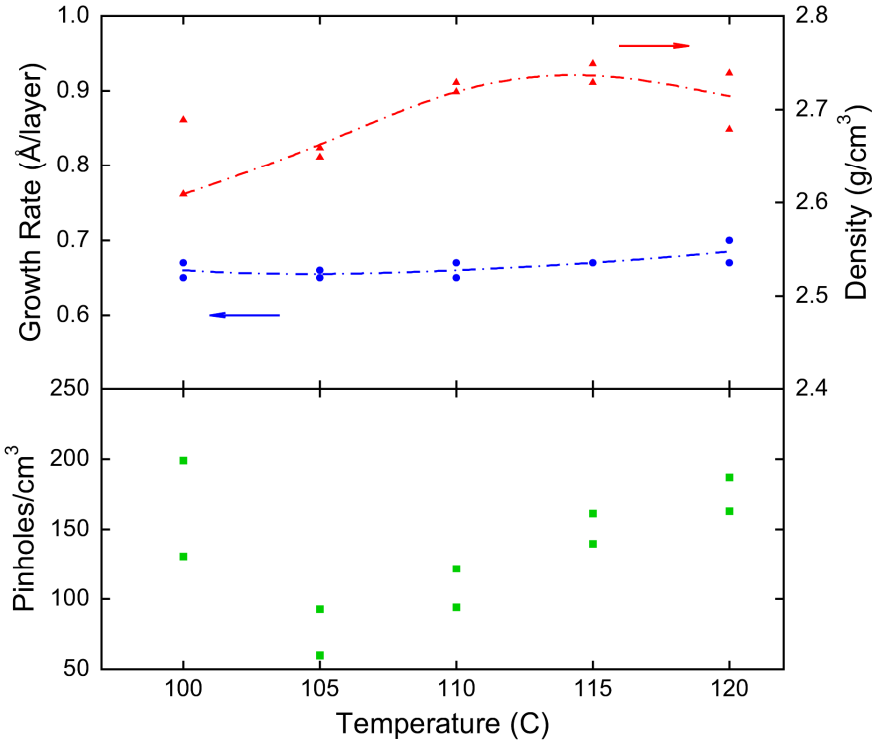

Figure 19 The growth rate per cycle, as well as the density and pinhole rate for 10 different samples as a function of deposition temperature.

Table 4

No. of Cycles	300	
Temperature	120	C
Precursor flow rate	1	SLPM
Purge flow rate	3	SLPM
TMA concentration	0.2	mol %
Water concentration	0.2	mol %
Substrate	ST504	

Finally, we looked at the effect of substrate speed on the film properties. Standard conditions are given in Table 4. The substrate speed was varied from .05 m/s to 1.0 m/s, and the results are shown in Fig. 20. At the higher speeds, the films were too thin to survive the sulfuric acid test,

so there are no pinhole data. We do see a low pinhole rate for extremely thick films, as we have seen in previous experiments.

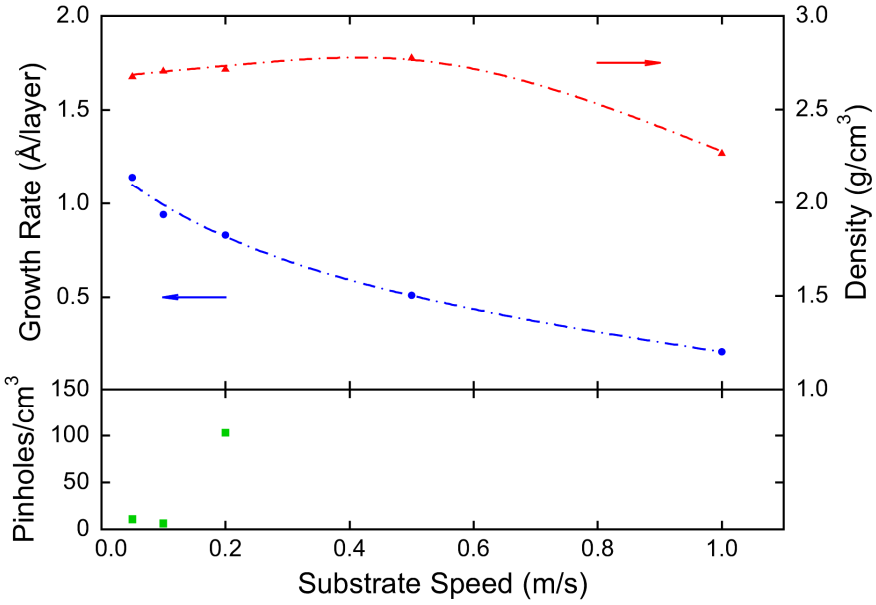

Figure 20 The growth rate per cycle, as well as the density and pinhole rate for 5 different samples as a function of substrate speed during deposition. The samples made at 0.5 m/s and 1.0 m/s were too damaged by the sulfuric acid test to allow pinhole counting.

If we look closely at the results of this experiment and the experiment on precursor flow rate, we can see a possible reason for the failure of this apparatus to produce high quality barrier films. The original modeling work was based on literature data for the kinetics of the precursor surface reaction rates and the diffusion constant for TMA in N_2 gas. These data indicated that the deposition kinetics would be extremely fast, and led to the current coating system design.

In Fig. 20, as the drum speed is reduced, the residence time increases, and so does the growth rate. We can define an effective exposure as the flow rate times the precursor concentration, and divided by the substrate speed. If the kinetics are fast enough that the residence time is unimportant, then samples made with similar exposures should be similar. The exposure for the sample made at 4 SLPM in Fig. 18 is equivalent to a substrate speed of 0.125 m/s in Fig. 20. Yet the growth rate in Fig. 18 is below 7 Å/cycle, while the growth rate implied by Fig. 20 for the same exposure is above 9 Å/cycle. In other words, the residence time *does* matter. At the higher, economically viable, substrate speeds, there is simply not enough time for the reaction to complete. In addition, the failure of the growth rate to saturate in Fig. 20 implies that the deposition does not have the expected characteristics of ALD, but rather has a large CVD (chemical vapor deposition) component.

The above interpretation of our experimental results is supported ESCA measurements. If the deposition is proceeding in part by CVD, then we expect molecular clusters formed by gas phase reactions between TMA and water to be incorporated into the film. These clusters would be characterized by OH groups, some of which do not react further and become buried in the film.

Such groups would result in films containing more oxygen than would be expected for stoichiometric Al_2O_3.

A total of five samples from the precursor ratio experiment were submitted for ESCA analysis, as summarized in Table 5.

Table 5

Sample	TMA Conc. (%)	H_2O Conc. (%)	Thickness (nm)
D102223-035	0.200	0.125	18
D102223-050	0.200	0.050	14
D102223-052	0.200	0.225	23
D102223-056	0.200	0.300	22

The figures below show the ESCA results for the four samples. The general trend is in fact that the O:Al ratio is above the stoichiometric expectation of 1.5. The effect is quite pronounced for the sample made at the lowest water concentration, and is more moderate for the remaining three samples.

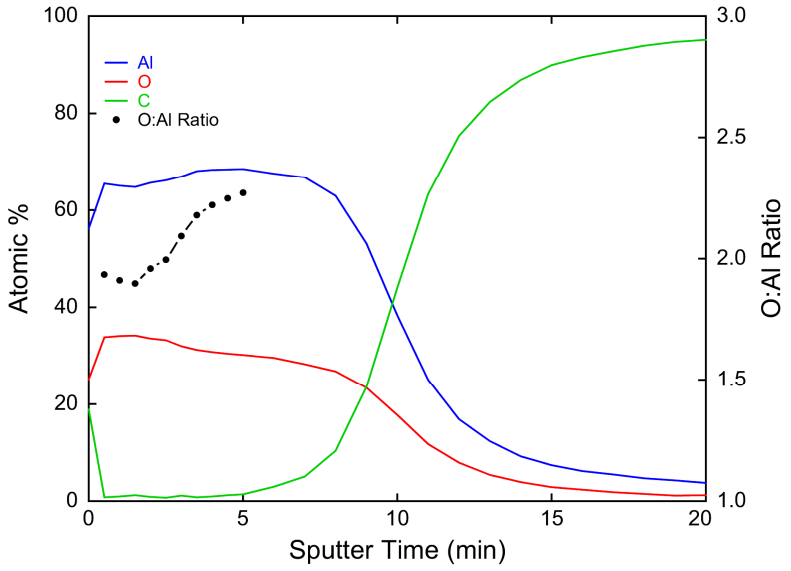

Figure 21 ESCA results for a film produced at a water concentration of 0.050%.

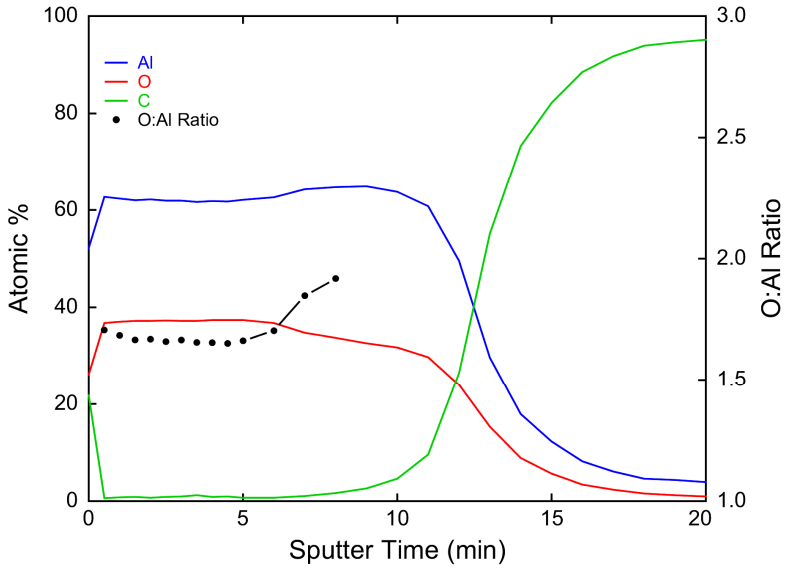

Figure 22 ESCA results for a film produced at a water concentration of 0.125%.

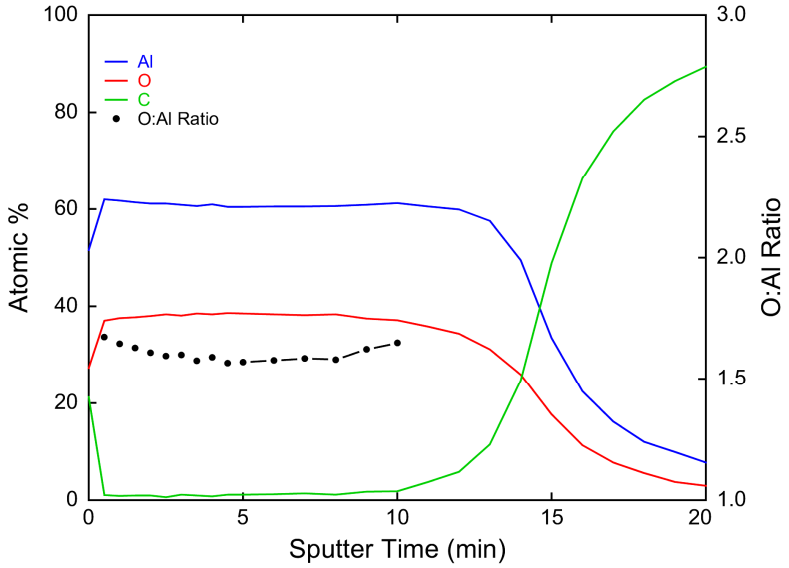

Figure 23 ESCA results for a film produced at a water concentration of 0.225%.

Fig. 25 shows the oxygen to aluminum ratio in more detail for all four samples. There are a couple of trends evident. The ratio is higher near the surface, and again at the interface with the PET substrate. In addition, the higher the water concentration, the closer the ratio becomes to 1.5.

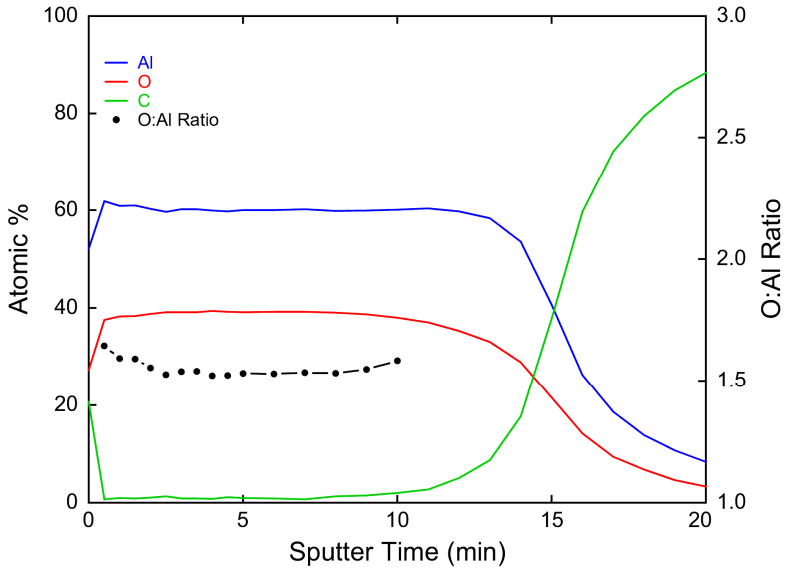

Figure 24 ESCA results for a film produced at a water concentration of 0.300%.

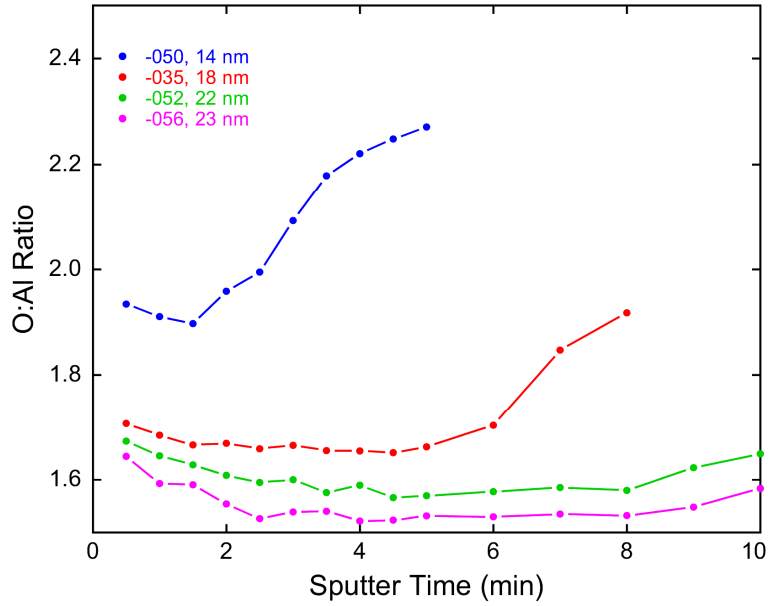

Figure 25 ESCA results for a film produced at a water concentration of 0.300%.

The ESCA analysis also revealed the presence of approximately 1% carbon throughout the thickness of the film. Fig. 26 shows that the carbon within the aluminum oxide is present in two forms: bonded with oxygen and bonded with hydrogen. The C-H signal could possibly be from

incompletely converted TMA. Alternatively, we could have some contamination from e.g. bearing oil, which might explain both carbon peaks.

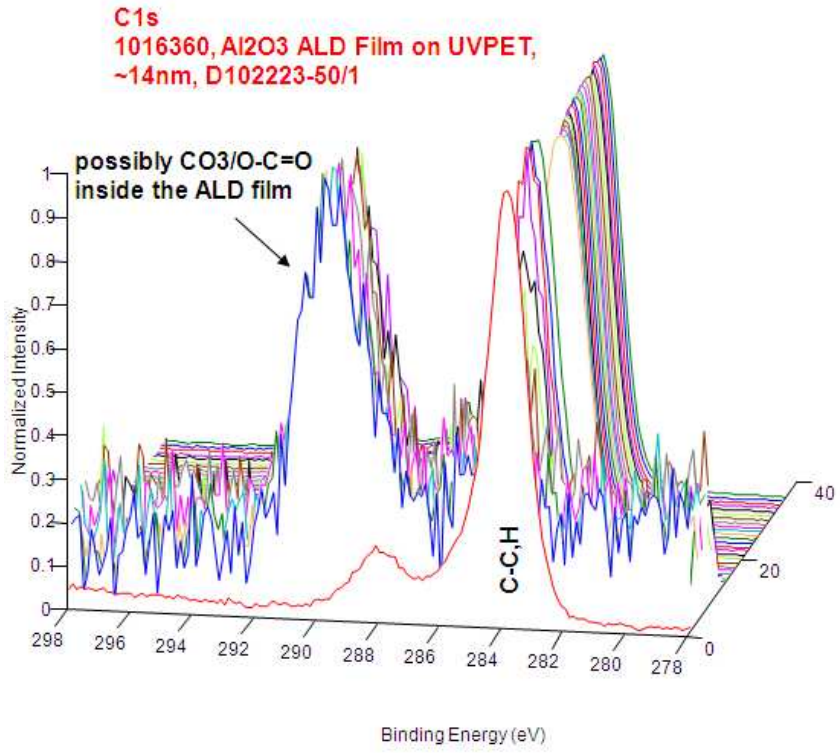

Figure 2H.1.1 Electron energy spectra for the carbon peaks observed in the ESCA analysis.

Conclusions

We designed and built a prototype apparatus for the continuous, high-speed deposition of ultrabarrier films at atmospheric pressure. The design was guided by numerical simulations which indicated that atomic layer deposition should be possible under these untested conditions. Unfortunately, the properties of the large number of samples produced do not support the original predictions. Instead, the data support two important conclusions:

1. Contrary to what was found in the model, this head design cannot prevent substantial mixing of the precursors in the gas phase, resulting in a film that is substantially formed by chemical vapor deposition, rather than atomic layer deposition.
2. The actual deposition rates are limited by kinetics, either gas phase transport, or surface reaction rates, that are well below what is expected based on the existing scientific literature.

While it is possible that additional work could yield a system design that produced films with the required properties, the current set of experiments does not point out a clear path to such a new design. Further progress will therefore require considerable theoretical and experimental effort.